Ultrasonics 84 (2018) 172–179

Contents lists available at ScienceDirect

Ultrasonics

journal homepage: www.elsevier.com/locate/ultras

A method for the design of ultrasonic devices for scanning acoustic microscopy using impulsive signals

Mototaka Arakawa [a,b,*], Hiroshi Kanai [b,a], Kazuo Ishikawa [b], Ryo Nagaoka [a], Kazuto Kobayashi [c], Yoshifumi Saijo [a,b]

[a] Graduate School of Biomedical Engineering, Tohoku University, Sendai 980-8579, Japan
[b] Graduate School of Engineering, Tohoku University, Sendai 980-8579, Japan
[c] Division of Research and Development, Honda Electronics, Co. Ltd., Toyohashi 441-3193, Japan

ARTICLE INFO

Article history:
Received 27 June 2017
Received in revised form 17 September 2017
Accepted 30 October 2017
Available online 2 November 2017

Keywords:
Scanning acoustic microscopy
Ultrasonic device
Loss
Frequency characteristic
Impulsive signal

ABSTRACT

Scanning acoustic microscopy (SAM) using impulsive signals is useful for characterization of biological tissues and cells. The operating center frequency of an ultrasonic device strongly depends on the performance characteristics of the device if the measurement is conducted by using impulsive signals. In this paper, a method for the design of ultrasonic devices for SAM using impulsive signals was developed. A new plane-wave model was introduced to calculate frequency characteristics of loss of ultrasonic devices by taking into account the conversion loss at the ultrasonic transducer, the transmission loss at the acoustic anti-reflection coating, and the propagation loss in the couplant. Ultrasonic devices were fabricated with a ZnO ultrasonic transducer using two acoustic lenses with aperture radii of 1.0 mm and 0.5 mm, respectively. The frequencies at which measured losses became minima corresponded to the calculation results by the plane-wave model. This numerical calculation method is useful for designing ultrasonic devices for acoustic microscopy using impulsive signals.

1. Introduction

Scanning acoustic microscopy (SAM) was developed to observe the microscopic region beneath the specimen surface of solids and biological tissues in the 1970 s [1–3]. To obtain higher-resolution images, higher-frequency ultrasonic devices have been developed [4]. Quantitative measurement methods of acoustic properties, such as velocity and attenuation coefficient, have also been developed to characterize biological tissues and cells. SAM has been applied for characterization of tissues or cells by measuring acoustic properties [5–10].

Rf burst signals are used as input signals for an ultrasonic transducer in conventional SAM. Acoustic images can be measured at arbitrary frequencies by setting the carrier frequency. However, it is impossible to separate the reflected signal from the front surface and that from the back surface for thin-sliced specimens if the round-trip propagation time in the specimen is shorter than the pulse width of the rf burst signal. In addition, it is time consuming to obtain two-dimensional distributions of acoustic properties because it is necessary to measure the reflected signals at several different frequencies with changing the carrier frequency of the rf burst signals at each measurement point [9,10].

On the other hand, SAM using impulsive signals has also been developed [11–16]. By using a high-frequency, broadband ultrasonic device, it is possible to distinguish the reflected signal from the front surface and that from the back surface of the thin specimens in the time domain. Thus, it is possible to obtain velocity of a specimen by measuring the difference of the arrival time of the signals. Saijo et al. developed a sound-speed microscope using impulsive signals for biological tissue and cell specimens [17–19]. However, it is difficult to distinguish two reflected signals for thin specimens with a thickness of several microns, even if impulsive signals are used in the measurements. In order to obtain acoustic properties of such thin specimens, a pulse spectrum method, which is an analysis procedure in the frequency domain of the superposed signals, was also developed [20–22]. However, in the measurements using impulsive signals, the operating center frequency and the bandwidth strongly depend on the performance characteristics of the ultrasonic device.

Ultrasonic devices for SAM have been designed based on the outcome of experimental measurement using rf burst signals. In the burst mode, measurements can be conducted at a desired frequency within the bandwidth of the ultrasonic device. Therefore, to obtain as high a resolution as possible, the operating center

* Corresponding author at: Graduate School of Biomedical Engineering, Tohoku University, Sendai 980-8579, Japan.
E-mail address: arakawa@ecei.tohoku.ac.jp (M. Arakawa).

https://doi.org/10.1016/j.ultras.2017.10.023
0041-624X/

frequency of the ultrasonic device is usually set to be higher than the frequency at which the loss of the device becomes minimum while taking the signal-to-noise ratio (S/N) into consideration. Otherwise, the operating center frequency and the bandwidth strongly depend on the operating characteristics of the ultrasonic device in measurements using the impulsive signals. Thus, the operating center frequency in the impulsive mode might be lower than the frequency that we expected based on the experience of the burst signals.

In this study, based on the results of numerical calculations and experiments, we evaluated performance characteristics of ultrasonic devices, viz., frequency characteristics of loss. A new procedure for the design and fabrication of ultrasonic devices for SAM was developed. Two fabricated ultrasonic devices were alternatively attached to a SAM, and two-dimensional distributions of intensity and velocity for a tissue specimen were measured as a demonstration.

2. A method for designing ultrasonic devices

2.1. Ultrasonic device

An acoustic lens or a concave transducer is usually used as the focusing device for SAM. The acoustic lens is mainly used in the frequency range above 100 MHz. Fig. 1 shows a cross-section of the ultrasonic device. An ultrasonic transducer is constructed on the plane surface of the rod having an acoustic lens. In order to obtain a narrow focused beam, material with high acoustic velocity should be selected for the rod. A *Z*-cut sapphire single crystal rod is normally used in frequency ranges higher than 100 MHz.

The focal length F of the acoustic lens is obtained by the following equation [23,24]:

$$F = \frac{R}{1 - \frac{V_C}{V_S}}, \tag{1}$$

where R is the curvature radius, and V_C and V_S are the velocities of liquid coupler and buffer rod, respectively. F is 1.15R when the coupler is water and the rod is a *Z*-cut sapphire.

The transmission coefficient from the sapphire rod to the water is very small because of the large difference of their acoustic impedances. Therefore, an acoustic anti-reflection coating (AARC) with a thickness of λ /4 (λ: wavelength) is normally formed on the aperture surface. All ultrasonic energies propagate from sapphire to water when the acoustic impedance of AARC Z_{AARC} has the following relationship:

$$Z_{AARC} = \sqrt{Z_S \cdot Z_C}, \tag{2}$$

where Z_S and Z_C are the acoustic impedance of the sapphire and that of the coupler, respectively.

Curvature radii R were designed as 1.0 mm around 225 MHz and 0.5 mm around 375 MHz based on experimental experiences of the measurements using rf tone burst pulses.

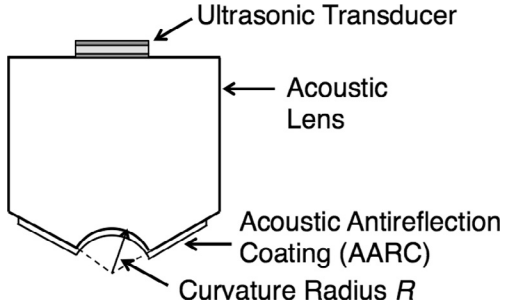

Fig. 1. Cross-section of the ultrasonic device for ultrasonic microscopy.

2.2. Factors of loss

As the factors of loss in the measurement using an acoustic lens, conversion loss (*CL*) from electric energy to mechanical energy at the ultrasonic transducer, propagation loss (*PL*) in the liquid coupler, and transmission loss (*TL*) at the AARC should be considered. Strictly speaking, the loss caused by focusing, e.g., aberration, should also be considered in the measurement using an acoustic lens. Here, we assumed that all ultrasonic energies emitted from the ultrasonic transducer converged at the focal point and returned to the ultrasonic transducer because two-dimensional scanning is conducted at the focal point of the ultrasonic device in the measurement of acoustic properties of biological tissues and cells. The total loss of the ultrasonic device was thus calculated as the product of *CL*, *TL*, and *PL* by the plane-wave model, which ignores the focusing effect. Diffraction loss caused by plane-wave propagation from the ultrasonic transducer with finite size, ultrasonic loss in the AARC, and electric loss at the electrode were also neglected.

2.3. Calculation method

CL was calculated by the method described in Ref. [25]. The velocity, thickness, and acoustic impedance of the piezoelectric material and the electrode, the electromechanical coupling factor and permittivity of the piezoelectric material, and the acoustic impedance of the acoustic lens were used in the calculation.

PL was calculated by the following equation.

$$PL = \exp(-2\alpha_C F), \tag{3}$$

where α_C is attenuation coefficient of the liquid coupler. The focal length F was obtained by Eq. (1) and α_C of the couplant such as water [26] or physiological saline solution [27] were obtained by the published data.

Reflection coefficient R_{ij} and transmission coefficient T_{ij} from medium i to medium j are expressed as follows:

$$R_{ij} = \frac{Z_j - Z_i}{Z_j + Z_i}, \tag{4}$$

$$T_{ij} = \frac{2Z_j}{Z_j + Z_i}. \tag{5}$$

Here, we assume media 1, 2, and 3 are the buffer rod, AARC, and the liquid coupler, respectively. The transmission coefficient from the buffer rod to the liquid coupler through AARC T_{13} and that from the liquid coupler to the buffer rod through AARC T_{31} are expressed as follows by assuming infinite reflections in AARC:

$$\begin{aligned} T_{13} &= T_{12}\cdot T_{23}\cdot\exp(-k_2 l_2) \\ &\quad + T_{12}\cdot R_{23}\cdot R_{21}\cdot T_{23}\cdot\exp(-3k_2 l_2) \\ &\quad + T_{12}\cdot R_{23}^2\cdot R_{21}^2\cdot T_{23}\cdot\exp(-5k_2 l_2)+\cdots \\ &= T_{12}\cdot T_{23}\cdot\exp(-k_2 l_2) \\ &\quad \times\{1 + R_{23}\cdot R_{21}\cdot\exp(-2k_2 l_2) \\ &\quad + R_{23}^2\cdot R_{21}^2\cdot\exp(-4k_2 l_2)+\cdots\} \\ &= (1+R_{12})\cdot(1+R_{23})\cdot\exp(-k_2 l_2) \\ &\quad \times\sum_{n=0}^{\infty}\{R_{23}\cdot R_{21}\cdot\exp(-2k_2 l_2)\}^n \\ &= (1+R_{12})\cdot(1+R_{23})\cdot\exp(-k_2 l_2) \\ &\quad \times\frac{1}{1 - R_{23}\cdot R_{21}\cdot\exp(-2k_2 l_2)} \\ &= \frac{(1+R_{12})\cdot(1+R_{23})\cdot\exp(-k_2 l_2)}{1 + R_{12}\cdot R_{23}\cdot\exp(-2k_2 l_2)}, \end{aligned} \tag{6}$$

$$T_{31} = \frac{(1+R_{32})\cdot(1+R_{21})\cdot\exp(-k_2 l_2)}{1 + R_{32}\cdot R_{21}\cdot\exp(-2k_2 l_2)}, \tag{7}$$

Table 1
Acoustic parameters used in the calculation.

Material	Velocity [m/s]	Density [kg/m^3]	Acoustic impedance $\times 10^6$ [kg/(m^{2}s)]	Attenuation coefficient [s^2/m]
Z-cut Sapphire	11217 [28]	3986 [28]	44.7	2.1×10^{-18} [29]
SiO_2 glass	5968 [30]	2200 [30]	13.1	1.3×10^{-16} [29]
Water	1491 [26]	998 [31]	1.5	2.23×10^{-14} [32]

Table 2
Acoustic parameters used in the calculation.

Material	Velocity [m/s]	Acoustic impedance $\times 10^6$ [kg/(m^{2}s)]	Electromechanical coupling factor	Permittivity [F/m]
Zinc Oxide	6330 [33]	36.0 [33]	0.24 [34]	7.8×10^{-11} [33]
Gold	3240 [30]	62.5 [30]	–	–

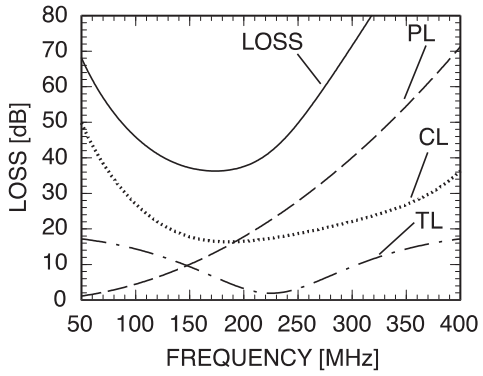

Fig. 2. Calculated result of loss of an ultrasonic device with $R = 1.0$ mm. The thickness of the ZnO transducer is 11.3 μm, and that of the SiO_2 AARC film is 6.63 μm.

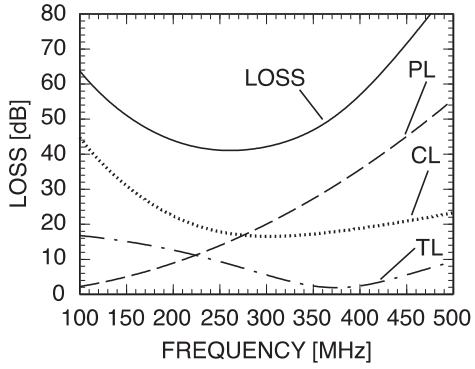

Fig. 3. Calculated result of loss of an ultrasonic device with $R = 0.5$ mm. The thickness of the ZnO transducer is 6.73 μm, and that of the SiO_2 AARC film is 3.98 μm.

where k_2 and l_2 are the wavenumber and length of AARC, respectively. *TL* was calculated by the following equation.

$$TL = T_{13} \cdot T_{31}. \tag{8}$$

2.4. Calculation

In the calculation, a *Z*-cut sapphire single crystal, SiO_2 glass, and water were assumed to be materials of the acoustic lens, the AARC, and the liquid coupler, respectively. We also assumed the following conditions. The ultrasonic transducer was composed of a ZnO thin film and gold electrodes. The aperture half angle was 60°. The size of the ultrasonic transducer was same as that of the aperture, and the diameter of the ultrasonic transducer was 1.73*R*. The parameters at room temperature used in the calculation are summarized in Tables 1 and 2.

At first, we calculated frequency characteristics of an ultrasonic device used around 225 MHz in the measurements using rf burst signals. Typical parameters are as follows: *R* is 1.0 mm, the thickness of ZnO is 11.3 μm, the thickness of gold electrode is 0.3 μm, and the thickness of SiO_2 AARC film is 6.63 μm. The frequency f_{AARC} at which *TL* became minimum was 225 MHz. The calculation results of loss are shown in Fig. 2. The dotted line, dashed line, and dashed-dotted line exhibit *CL*, *PL*, and *TL*, respectively. We calculated round-trip losses because the measurements were conducted in the reflection mode. The total loss (*LOSS*) was obtained as the product of *CL*, *PL*, and *TL*. *CL* was minimum at 186 MHz, smaller than 280 MHz of λ /2 resonance frequency of the ultrasonic transducer because of the high acoustic impedance of sapphire and the complex resonance of the ultrasonic transducer consisting of a ZnO transducer and gold electrodes. *PL* is the main factor of *LOSS* in the higher-frequency region because it is proportional to the square of frequency. The minimum *LOSS* was 36.3 dB at 173 MHz, and the frequency was 52 MHz less than the frequency at which *TL* was minimum. The calculated results suggested that the operating center frequency in the measurements using impulsive signals became smaller than the frequency at which *TL* was minimum because *CL* and *PL* also affect the total loss.

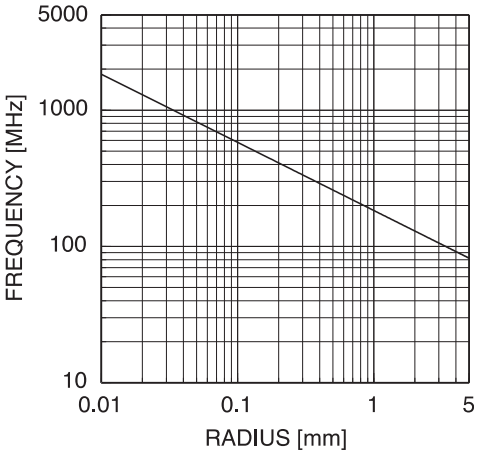

Fig. 4. Relationship between curvature radius and frequency in the case that the propagation loss in the water coupler is 15 dB.

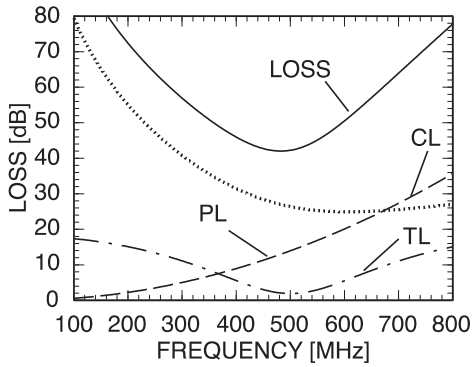

Fig. 5. Calculated result of loss of an ultrasonic device with $R = 0.125$ mm. The thickness of the ZnO transducer is 3.33 μm, and that of the SiO_2 AARC film is 2.98 μm.

Table 3
Parameters of ultrasonic devices.

		No. 1	No. 2
Lens	Material	*Z*-cut Sapphire	*Z*-cut Sapphire
	Diameter of rod	6 mm	6 mm
	Length of rod	5.5 mm	3 mm
	Radius of aperture	1 mm	0.5 mm
	Half angle of aperture	60°	60°
Transducer	Material	ZnO	ZnO
	Thickness	12.66 μm	6.33 μm
Electrode	Material	Au-Cr	Au-Cr
	Diameter	1.73 mm	0.87 mm
	Thickness	0.3 μm	0.3 μm
AARC	Material	SiO_2 glass	SiO_2 glass
	Thickness	7.46 μm	4.97 μm

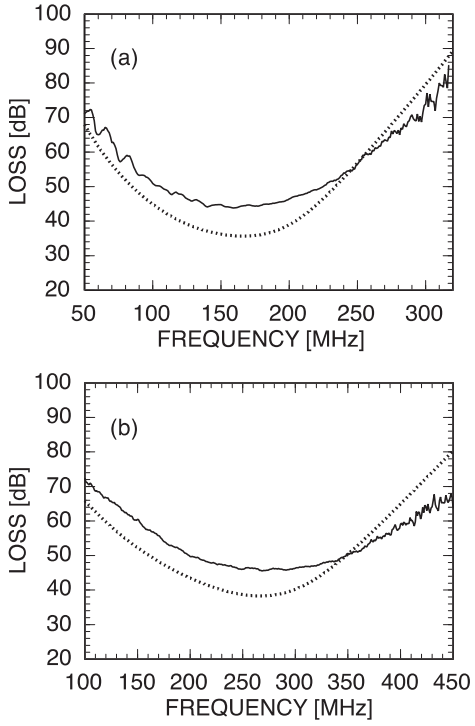

Fig. 6. Comparisons between measured and calculated losses of the PFB ultrasonic devices. Solid lines: measured. Dotted lines: calculated. (a) Device 1 ($R = 1.0$ mm). (b) Device 2 ($R = 0.5$ mm).

Table 4
Minimum losses of the point-focus-beam ultrasonic devices. The frequencies in the parenthesis are the frequencies at which the losses became minimum.

Device	Measured	Calculated
No. 1	43.8 dB (159 MHz)	35.7 dB (166 MHz)
No. 2	45.6 dB (268 MHz)	38.3 dB (267 MHz)

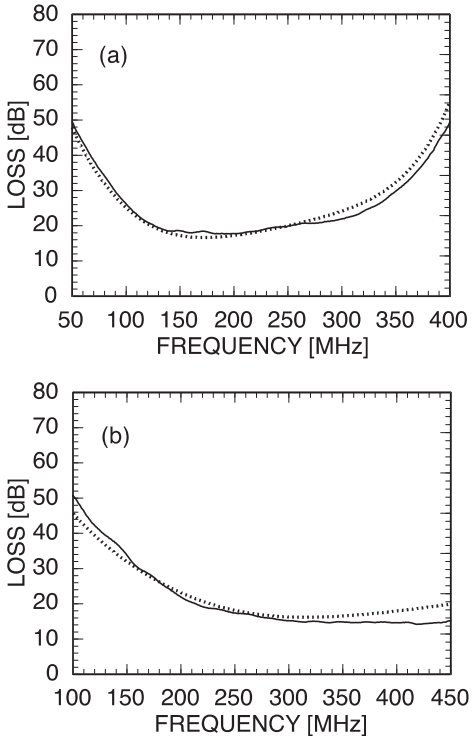

Fig. 7. Comparisons of measured and calculated results of losses of the plane-wave ultrasonic devices. Solid lines: measured. Dotted lines: calculated. (a) Device 1P. (b) Device 2P.

Next, we calculated the frequency characteristics of an ultrasonic device used around 375 MHz in measurements using rf burst signals. Typical parameters are as follows: R is 0.5 mm, the thickness of ZnO is 6.73 μm, the thickness of gold electrode is 0.3 μm, and the thickness of SiO_2 AARC film is 3.98 μm ($f_{AARC} = 375$ MHz). The calculation results are shown in Fig. 3. *CL* was minimum at 303 MHz, and minimum *LOSS* was 41.1 dB at 261 MHz. The operating center frequency was 114 MHz less than desired. From Figs. 2 and 3, the operating center frequencies were lower than the frequency at which *TL* was minimum we set based on the experimental experiences in the burst mode.

2.5. Design methodology

The frequencies at which *LOSS* became minimum were less than the frequency at which *CL* and *TL* became minimum in Figs. 2 and 3. These results were mainly caused by the large propagation loss in the liquid coupler (water). In Figs. 2 and 3, propagation losses were 13.3 dB and 15.2 dB at the frequencies at which *LOSS* became minimum, respectively. Meanwhile, they were 22.6 dB and 31.3 dB at the frequencies at which *TL* became minimum for devices No. 1 and No. 2, respectively. Therefore, the curvature radius of the acoustic lens should be determined so that propagation loss in the coupler is around 15 dB at the operating center frequency.

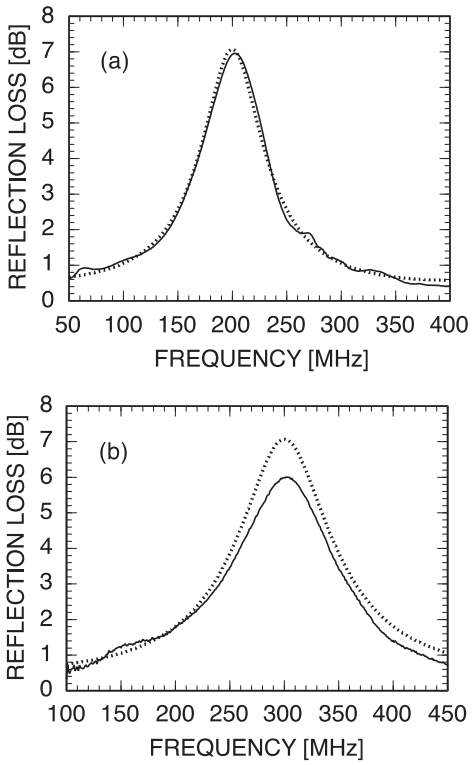

Fig. 8. Comparisons of measured and calculated results of the reflection losses of the plane-wave ultrasonic devices. Solid lines: measured. Dotted lines: calculated. (a) Device 1P. (b) Device 2P.

Table 5
Minimum losses and maximum reflection losses of the plane-wave ultrasonic devices. The frequencies in the parenthesis are the frequencies at which the losses became minimum or the reflection losses became maximum.

Device		Measured	Calculated
No. 1P	Minimum loss	17.7 dB (191 MHz)	16.7 dB (172 MHz)
	Maximum reflection loss	7.0 dB (203 MHz)	7.1 dB (200 MHz)
No. 2P	Minimum loss	14.2 dB (418 MHz)	16.2 dB (316 MHz)
	Maximum reflection loss	6.0 dB (302 MHz)	7.1 dB (300 MHz)

Fig. 4 indicates the relationship between the curvature radius of the acoustic lens and the frequency at which *PL* calculated by Eqs. (1) and (3) became 15 dB. From Fig. 4, the frequencies were calculated as 183 MHz and 259 MHz for $R = 1$ mm and 0.5 mm, respectively.

Next, we demonstrated the procedure to design ultrasonic devices by calculating *LOSS* of a device with an operating center frequency of 500 MHz. First, the curvature radius was obtained as 0.125 mm from Fig. 4. The diameter of the ultrasonic transducer became 0.22 mm from the aperture half angle of 60°. The focal length *F* was calculated by Eq. (1), and *AL* was calculated by Eq. (4). The thickness of SiO_2 AARC was determined to be 2.98 μm so that f_{AARC} became 500 MHz. *TL* was calculated by Eq. (8). The thickness of ZnO was determined to minimize *LOSS* at the operating center frequency by calculating *CL* with changing the thickness. Fig. 5 shows the calculated loss in the case that the thickness of ZnO was 3.33 μm and that of the gold electrode was 0.2 μm. *LOSS* was a minimum of 42.0 dB at 483 MHz. So, ultrasonic devices with the desired operating center frequency could be designed by using this method.

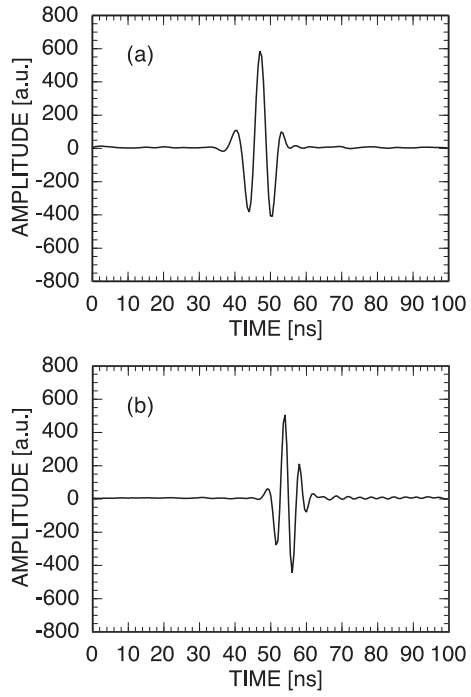

Fig. 9. Reflected signals from the surface of a slide glass. (a) Device 1. (b) Device 2.

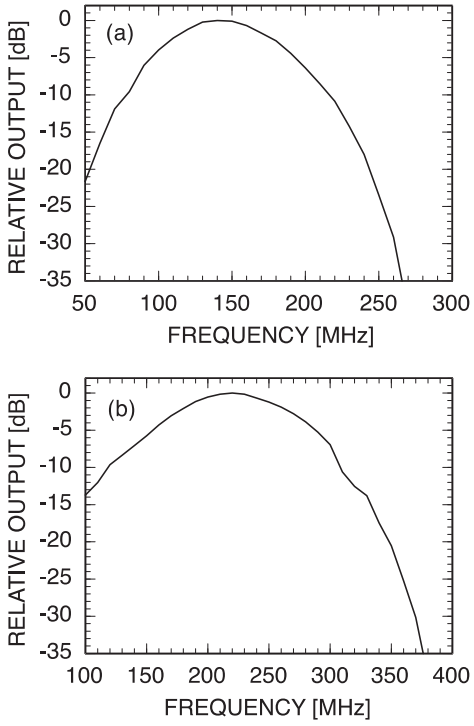

Fig. 10. Frequency characteristics of the reflected signals shown in Fig. 9 obtained by FFT analysis. (a) Device 1. (b) Device 2.

3. Experiments and discussion

Point-focus-beam (PFB) ultrasonic devices No. 1 and No. 2 were fabricated using acoustic lenses with $R = 1.0$ mm and $R = 0.5$ mm, respectively. Parameters of the devices are shown in Table 3. Taking the numerical calculation results in Sec. 2 into account, the thicknesses of SiO_2 AARC were determined to be 7.46 μm

(f_{AARC} = 200 MHz) for device No. 1 and 4.97 μm (f_{AARC} = 300 MHz) for device No. 2. Thicknesses of ZnO film were 12.66 μm for No. 1 and 6.33 μm for No.2, which were optimized to minimize minimum *LOSS*. To investigate the factors of loss experimentally, plane-wave (PW) ultrasonic devices No. 1P and No. 2P were also fabricated with the same parameters as those of the PFB devices No. 1 and No. 2, respectively, by using cylindrical rods with a diameter of 6 mm and a length of 6 mm instead of acoustic lenses.

The fabrication procedure of the ultrasonic devices was as follows. First, the acoustic lens was cleaned with organic solvents by ultrasonic bath. Then, SiO_2 AARC film was deposited on the lens surface by rf sputtering. Next, Au-Cr film was deposited on the plane surface by vacuum evaporation, ZnO film was deposited by dc sputtering [34], and Au-Cr film was again deposited. Then, the lens was inserted into a stainless holder, an SMA connector was attached to the holder, and copper wires were used to connect the electrodes and the connector.

Frequency characteristics of loss of the devices were measured by the pulse mode measurement system [35]. The input peak-to-peak voltage to the ultrasonic transducer was less than 2.8 V. The pulse widths of the rf tone burst pulses were 350 ns and 250 ns for the devices 1 and 2, respectively. The pulse

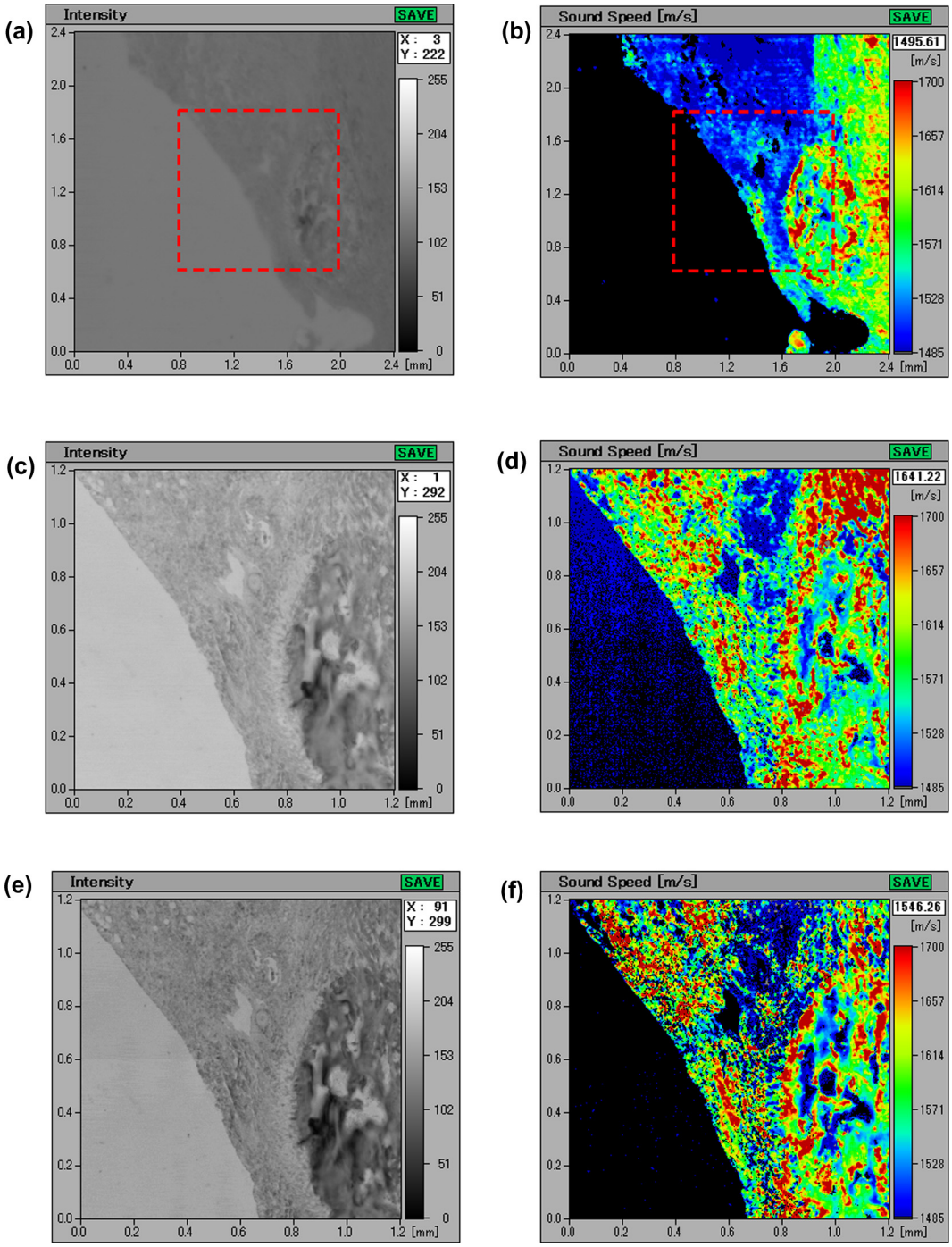

Fig. 11. Measured intensities and velocities for tendon tissue of the left leg of an S-D rat. (a) Intensity by 80-MHz device. (b) Velocity for 80-MHz device. (c) Intensity by device No. 1. (d) Velocity by device No. 1. (e) Intensity by device No. 2. (f) Velocity by device No. 2.

repetition frequency was set to 1 kHz taking into account reverberations in the acoustic lens. Water and a synthetic silica (SiO_2) glass substrate were used as the coupler and the reflector, respectively. The glass surface was set at the focal point of the PFB ultrasonic device. The input power to the ultrasonic device and the output power of the reflected signal from the glass surface were measured, and loss was obtained by the ratio of these signals. The results are shown in Fig. 6. The reflection loss from the coupler to the reflector was calculated as 2.0 dB from their acoustic impedances, and it was added to the calculation results. Minimum values of losses and the frequencies at which the losses became minimum are summarized in Table 4. The frequencies at which the losses became minimum in the measured loss almost coincided with the calculated values for both devices. These frequencies were also close to the frequencies of 183 MHz and 259 MHz at which *PL* became 15 dB. 6-dB bandwidths were 116 MHz (73%) for No. 1 and 170 MHz (63%) for No. 2, and it was possible to obtain a sufficient bandwidth for the pulse drive.

Next, we experimentally discuss factors of loss of the PFB ultrasonic device. We also measured conversion loss at the ultrasonic transducer and reflection loss at the AARC for PW devices No. 1P and No. 2P. Conversion loss was obtained by measuring the input power to ultrasonic transducers and the output power of a signal reflected from the opposite end of the buffer rod. Reflection loss at the AARC was obtained by measuring the output powers of the signals reflected from the opposite end of the buffer rod without and with water [36]. The results are shown in Figs. 7 and 8. Minimum values of the conversion loss and the frequencies at which the conversion losses became minimum, and maximum values of the reflection loss and the frequencies at which the reflection losses became maximum are shown in Table 5. The measured conversion loss and reflection loss almost corresponded to the calculated values for devices No. 1P and No. 2P. Therefore, *CL* and *TL* of PFB ultrasonic devices No. 1 and No. 2 should have almost coincided with the calculated values. The attenuation coefficient of water was obtained from published data [32]. Therefore, the differences between the measured and calculated losses of the PFB ultrasonic devices No. 1 and No. 2 were considered to be caused by the effect of the focused beam. Particularly, aberration of the acoustic lens was considered to be the main factor. Transmission coefficient at the AARC is different from the position of lens because of the thickness distribution ($l_2 \cdot \cos\theta$, θ : incident angle) caused by the fabrication process, and it was also considered to affect the frequency characteristics. However, the frequencies at which the measured losses became minimum corresponded to the calculated values. Thus, the calculation method using the plane-wave model is indicated to be useful for designing PFB ultrasonic devices with a desired operating center frequency for the pulse signal.

4. Application

PFB ultrasonic devices No. 1 and No. 2 were attached to a medical SAM (AMS-50SI, Honda Electronics, Co. Ltd.) and driven by impulsive signals. The focal point of the device was set at the surface of the slide glass. Reflected signals from the front surface of the slide glass in the time domain are shown in Fig. 9. The frequency spectra obtained by fast Fourier transform (FFT) of Fig. 9 are shown in Fig. 10. The pulse widths were narrow and the frequency characteristics were wide. The operating center frequencies in Fig. 10 were lower than those in Fig. 6, because the results in Fig. 10 were not normalized by the frequency characteristics of the input pulse, which has frequency characteristic that drops as the frequency increases [18].

Next, a Sprague-Dawley (SD) rat was taken as a specimen. The tendon tissue of left leg was sliced and mounted on a slide glass. Two-dimensional distributions of intensity and velocity were measured with PFB ultrasonic devices No. 1 and No. 2, and a concave transducer with a center frequency of 80 MHz [18]. The results are shown in Fig. 11. First, two-dimensional measurements were conducted in 8-μm steps for an area of 2.4 mm × 2.4 mm by using a 80-MHz concave transducer. Then, two-dimensional measurements were conducted in 4-μm steps with an area of 1.2 mm × 1.2 mm indicated by the red dashed lines in Fig. 11(a) and (b) by using devices No. 1 and No. 2. Similar results were obtained by all devices because of sufficient S/N. As the center frequency of the ultrasonic device was higher, the spatial resolution in acoustic image became higher. Similar results were obtained in velocity distributions for each device. The fabricated ultrasonic devices had sufficient amplitude and bandwidth for measurement of biological tissues.

5. Conclusions

In this study, we examined frequency characteristics of ultrasonic devices for SAM using impulsive signals by numerical calculations and experiments. We developed a new method to calculate the loss of ultrasonic devices by the plane-wave model, taking into consideration the conversion loss at the ultrasonic transducer, the propagation loss in the liquid coupler, and the transmission loss at the AARC. We first calculated frequency characteristics of the ultrasonic device used in the measurements in the burst mode. We clarified that the operating center frequency of the ultrasonic device in the impulsive mode was lower than the expected value if the device was designed by the experimental experiences in the burst mode. From the results, we developed a procedure to design the ultrasonic device, taking the propagation loss in the coupler at the operating center frequency into consideration. Next, we fabricated ultrasonic devices with a ZnO transducer using acoustic lenses with $R = 1.0$ mm and $R = 0.5$ mm. By comparing the measured losses with the calculated results, the frequencies at which the loss becomes minimum in the measured loss almost coincided with the calculated values for both devices, although the values were different. Then, the ultrasonic devices were installed in a medical SAM, and measurements of ultrasonic images and acoustic properties of tissue specimens were successfully demonstrated. Therefore, this numerical calculation method is indicated to be useful for designing ultrasonic devices for SAM using impulsive signals. Of course, this method is also useful for designing ultrasonic devices for the burst mode.

As a next step, we will fabricate devices with higher operating center frequencies and apply them to measurement of the acoustic properties of cells.

References

[1] A. Korpel, L.W. Kessler, P.R. Palermo, Acoustic microscope operating at 100 MHz, Nature 232 (1971) 110–111.
[2] R.A. Lemons, C.F. Quate, A Scanning acoustic microscope, Proc. 1973, IEEE Ultrason. Symp (1973) 18–21.
[3] R.A. Lemons, C.F. Quate, Acoustic microscopy: biomedical applications, Science 188 (1975) 905–911.
[4] V. Jipson, C.F. Quate, Acoustic microscopy at optical wavelength, Appl. Phys. Lett. 32 (1978) 789–791.
[5] J.A. Hildebrand, D. Rugar, Measurement of cellular elastic properties by acoustic microscopy, J. Microsc. 134 (1984) 245–260.
[6] H. Lüers, K. Hillmann, J. Litniewski, J. Bereiter-Hahn, Acoustic microscopy of cultured cells Distribution of forces and cytoskeletal elements, Cell Biophys. 18 (1991) 279–293.
[7] A. Kinoshita, S. Senda, K. Mizushige, H. Masugata, S. Sakamoto, H. Kiyomoto, H. Matsuo, Evaluation of acoustic properties of the live human smooth-muscle cell using scanning acoustic microscopy, Ultrasound Med. Biol. 24 (1998) 1397–1405.

[8] T. Kundu, J. Bereiter-Hahn, I. Karl, Cell property determination from the acoustic microscope generated voltage versus frequency curves, Biophys. J. 78 (2000) 2270–2279.
[9] Y. Saijo, M. Tanaka, H. Okawai, F. Dunn, The ultrasonic properties of gastric cancer tissues obtained with a scanning acoustic microscope system, Ultrasound Med. Biol. 17 (1991) 709–714.
[10] Y. Saijo, M. Tanaka, H. Okawai, H. Sasaki, S. Nitta, F. Dunn, Ultrasonic tissue characterization of infarcted myocardium by scanning acoustic microscopy, Ultrasound Med. Biol. 23 (1997) 77–85.
[11] G.A.D. Briggs, J. Wang, R. Gundle, Quantitative acoustic microscopy of individual living human cells, J. Microsc. 172 (1993) 3–12.
[12] R.M. Lemor, E.C. Weiss, G. Pilarczyk, P.V. Zinin, Mechanical properties of single cells - measurement possibilities using time-resolved scanning acoustic microscopy, Proc. 2004, IEEE Int. Ultrasonics, Ferroelectr., Freq. Control (2004) 622–629.
[13] P.V. Zinin, P. Anastasiadis, E.C. Weiss, R.M. Lemor, Variation of the sound attenuation inside HeLa cells during cell division using high-frequency time-resolved acoustic microscope, Proc. 2007, IEEE Int. Ultrasonics Symp (2007) 813–816.
[14] E.C. Weiss, P. Anastasiadis, G. Pilarczyk, R.M. Lemor, P.V. Zinin, Mechanical properties of single cells by high-frequency time-resolved acoustic microscopy, IEEE Trans. Ultrason., Ferroelectr., Freq. Contr 54 (2007) 2257–2271.
[15] E.M. Strohm, M.C. Kolios, Measuring the mechanical properties of cells using acoustic microscopy, Proc. 31st Annu. Int. Conf. IEEE Eng. Med. Biol. Soc. (2009) 6042–6045.
[16] E.M. Strohm, G.J. Czarnota, M.C. Kolios, Quantitative measurements of apoptotic cell properties using acoustic microscopy, IEEE Trans. Ultrason., Ferroelectr., Freq. Contr 57 (2010) 2293–2304.
[17] Y. Saijo, N. Hozumi, C. Lee, M. Nagao, K. Kobayashi, N. Okada, N. Tanaka, E.S. Filho, H. Sasaki, M. Tanaka, T. Yambe, Ultrasonic speed microscopy for imaging of coronary artery, Ultrasonics 44 (2006) e51–e55.
[18] Y. Saijo, E.S. Filho, H. Sasaki, T. Yambe, M. Tanaka, N. Hozumi, K. Kobayashi, N. Okada, Ultrasonic tissue characterization of atherosclerosis by a speed-of-sound microscanning system, IEEE Trans. Ultrason., Ferroelectr., Freq. Contr 54 (2007) 1571–1577.
[19] M. Arakawa, J. Shikama, K. Yoshida, R. Nagaoka, K. Kobayashi, Y. Saijo, Development of an ultrasonic microscope combined with optical microscope for multiparametric characterization of a single cell, IEEE. Trans. Ultrason., Ferroelectr., and Freq. Contr. 62 (2015) 1615–1621.
[20] N. Hozumi, R. Yamashita, C.-K. Lee, M. Nagao, K. Kobayashi, Y. Saijo, M. Tanaka, N. Tanaka, S. Ohtsuki, Ultrasonic sound speed microscope for biological tissue characterization driven by nanosecond pulse, Acoust. Sci. & Tech. 24 (2003) 386–390.
[21] K. Miura, H. Nasu, S. Yamamoto, Scanning acoustic microscopy for characterization of neoplastic and inflammatory lesions of lymph nodes, Sci. Rep. 3 (2013) 1255.
[22] K. Miura, S. Yamamoto, A scanning acoustic microscope discriminates cancer cells in fluid, Sci. Rep. 5 (2015) 15243.
[23] R.A. Lemons and C.F. Quate, "Acoustic microscopy," Physical Acoustics XIV (Ed. W. P. Mason and R. N. Thurston), Academic Press, London, (1979) 20–21.
[24] G.A.D. Briggs, O.V. Kolosov, Acoustic microscopy, Oxford University Press, Oxford, 1979, pp. 13–14.
[25] Y. Kikuchi, N. Chubachi, S. Yamamizu, Analysis of ultrasonic multi-layer transducer for UHF and VHF ranges, J. IEICE Trans. A 55-A (1972) 331–338.
[26] W. Kroebel, K.-H. Mahrt, Recent results of absolute sound velocity measurements in pure water and sea water at atmospheric pressure, Acustica 35 (1976) 154–164.
[27] J.C. Carman, Classroom measurements of sound speed in fresh/saline water, J. Acoust. Soc. Am. 131 (2012) 2455–2458.
[28] M. Arakawa, J. Kushibiki, Y. Madani, Ultrasonic micro-spectroscopy of synthetic sapphire crystals, Jpn. J. Appl. Phys. 47 (2008) 2285–2287.
[29] B.A. Auld, Acoustic fields and waves in solids, John Wiley & Sons, New York, 1973, p. 96.
[30] W.P. Mason, Physical Acoustics and the Properties of Solids, McGraw-Hill, New York, 1958, pp. 17–20.
[31] F.E. Jones, G.L. Harris, ITS-90 density of water formulation for volumetric standards calibration, J. Res. Nat. Inst. Stand. Tech. 97 (1992) 335–340.
[32] Y. Hashimoto, N. Akashi, J. Kushibiki, Measurements of ultrasonic attenuation coefficients of water in VHF/UHF range, Tech. Rep. IEICE 97 (1997) 37–42.
[33] N.F. Foster, G.A. Coquin, G.A. Rozgonyi, F.A. Vannatta, Cadmium sulphide and zinc oxide thin-film transducers, IEEE Trans. Son. Ultrason. SU- 15 (1968) 28–41.
[34] N. Chubachi, M. Minakata, Y. Kikuchi, Physical structure of DC diode sputtered ZnO films and its influence on the effective electromechanical coupling factors, Jpn. J. Appl. Phys. Suppl. 2 (Pt. 1) (1974) 737–740.
[35] J. Kushibiki, T. Sannomiya, N. Chubachi, A useful acoustic measurement system for pulse mode in VHF and UHF ranges, IEEE Trans. Son. Ultrason. SU- 29 (1982) 338–342.
[36] J. Kushibiki, H. Maehara, N. Chubachi, Acoustic properties of evaporated chalcogenide glass films, Electron. Lett. 17 (1981) 322–323.